Unique dynamics and exocytosis properties of GABAergic synaptic vesicles revealed by three-dimensional single vesicle tracking

Chungwon Park[a] , Xingxiang Chen[a] , Chong-Li Tian[b,c], Gyu Nam Park[d,e], Nicolas Chenouard[f], Hunki Lee[a,g], Xin Yi Yeo[h,i], Sangyong Jung[h,j] , Richard W. Tsien[k,1] , Guo-Qiang Bi[b,c] , and Hyokeun Park[a,l,m,1]

[a]Division of Life Science, The Hong Kong University of Science and Technology, Clear Water Bay, 999077 Kowloon, Hong Kong; [b]School of Life Sciences, University of Science and Technology of China, Hefei, 230052 Anhui, China; [c]Chinese Academy of Sciences, Key Laboratory of Brain Function and Disease, University of Science and Technology of China, Hefei, 230052 Anhui, China; [d]Department of Chemistry, Chung-Ang University, 06974 Seoul, Korea; [e]Creative Research Initiative Center for Chemical Dynamics in Living Cells, Chung-Ang University, 06974 Seoul, Korea; [f]CNRS, Interdisciplinary Institute for Neuroscience, IINS, UMR 5297, University of Bordeaux, F-33000 Bordeaux, France; [g]Institute of Medical Physics and Biophysics, University of Münster, 48149 Münster, Germany; [h]Singapore Bioimaging Consortium, Agency for Science, Technology, and Research, 138667 Singapore; [i]Department of Psychological Medicine, Yong Loo Lin School of Medicine, National University of Singapore, 117597 Singapore; [j]Department of Physiology, Yong Loo Lin School of Medicine, National University of Singapore, 117597 Singapore; [k]Department of Neuroscience and Physiology, New York University Neuroscience Institute, New York University, New York, NY 10016; [l]Department of Physics, The Hong Kong University of Science and Technology, Clear Water Bay, 999077 Kowloon, Hong Kong; and [m]State Key Laboratory of Molecular Neuroscience, The Hong Kong University of Science and Technology, Clear Water Bay, 999077 Kowloon, Hong Kong

Maintaining the balance between neuronal excitation and inhibition is essential for proper function of the central nervous system. Inhibitory synaptic transmission plays an important role in maintaining this balance. Although inhibitory transmission has higher kinetic demands compared to excitatory transmission, its properties are poorly understood. In particular, the dynamics and exocytosis of single inhibitory vesicles have not been investigated, due largely to both technical and practical limitations. Using a combination of quantum dots (QDs) conjugated to antibodies against the luminal domain of the vesicular GABA transporter to selectively label GABAergic (i.e., predominantly inhibitory) vesicles together with dual-focus imaging optics, we tracked the real-time three-dimensional position of single GABAergic vesicles up to the moment of exocytosis (i.e., fusion). Using three-dimensional trajectories, we found that GABAergic synaptic vesicles traveled a shorter distance prior to fusion and had a shorter time to fusion compared to synaptotagmin-1 (Syt1)-labeled vesicles, which were mostly from excitatory neurons. Moreover, our analysis revealed that GABAergic synaptic vesicles move more straightly to their release sites than Syt1-labeled vesicles. Finally, we found that GABAergic vesicles have a higher prevalence of kiss-and-run fusion than Syt1-labeled vesicles. These results indicate that inhibitory synaptic vesicles have a unique set of dynamics and exocytosis properties to support rapid synaptic inhibition, thereby maintaining a tightly regulated coordination between excitation and inhibition in the central nervous system.

synaptic vesicles | dynamics | exocytosis | three-dimensional tracking | inhibitory synaptic transmission

Neurons communicate with other neurons by releasing neurotransmitters from their presynaptic terminals via the exocytosis (i.e., fusion) of synaptic vesicles at the presynaptic membrane, subsequently activating postsynaptic receptors to mediate downstream effects (1–4). Synapses in the central nervous system can be broadly classified as either excitatory or inhibitory, depending on the type of neurotransmitters that they release and the effects of those neurotransmitters. While excitatory synapses cause the generation, propagation, and potentiation of neuronal responses for processing information (5), inhibitory synapses play an essential role in feedback and feedforward inhibition in order to control neural excitability (6) and in the control of brain rhythms (7). In the central nervous system, inhibitory synaptic transmission is mediated primarily by release of the neurotransmitter GABA and serves to coordinate the pattern of excitation and the

synchronization of the neuronal network, thereby regulating neuronal excitability (8, 9). Thus, maintaining a tightly regulated coordination between excitatory and inhibitory neurotransmission is essential for proper brain function.

An extensive analysis of the components and molecular events involved in vesicle fusion and neurotransmitter release has yielded general models describing the organization and functional properties of both presynaptic and postsynaptic components (10–12). On the presynaptic side, a transient increase in local Ca^{2+} concentration due to activation of voltage-gated Ca^{2+} channels triggers the localized buckling of the plasma membrane via a direct interaction between the C2B domain in the protein synaptotagmin-1 (Syt1) and lipids in the membrane (13–15). This leads to the synchronous fusion between the synaptic vesicles and the plasma membrane and release of the vesicle's contents into the synaptic cleft (16), enabling excitatory and inhibitory neurotransmitters to

Significance

Despite playing an important role in maintaining brain function, the dynamics and exocytosis of inhibitory synaptic vesicles are poorly understood. Here, we tracked the three-dimensional position of single GABAergic vesicles up to the moment of exocytosis in real time by loading single GABAergic vesicles with quantum dots conjugated to antibodies against the luminal domain of the vesicular GABA transporter. We found that GABAergic synaptic vesicles have a smaller total travel length before fusion, a shorter fusion latency, and a higher prevalence of kiss-and-run fusion than synaptotagmin-1–labeled vesicles. Our findings provide evidence that inhibitory vesicles have a unique set of dynamics and exocytosis properties to support rapid inhibitory synaptic transmission.

www.manaraa.com

diffuse to and act upon postsynaptic glutamate and GABA receptors, respectively.

Importantly, our general understanding of neurotransmitter release stems from studying excitatory neurotransmission and is currently unable to adequately explain the distinct features associated with inhibitory synaptic transmission. For example, the size of the readily releasable pool (RRP) of synaptic vesicles in striatal inhibitory GABAergic neurons—probed by a hypertonic sucrose solution—is three times larger than the RRP in excitatory hippocampal glutamatergic neurons (17). Furthermore, inhibitory neurons have both higher average vesicular release probability (P_r) and more release sites compared to excitatory neurons (17–19). These results suggest that quantitative differences exist between inhibitory and excitatory synapses with respect to vesicle dynamics, release, and recycling. In addition, disproportionate effects between inhibitory and excitatory synapses following knockout of some or all synapsin genes provide a molecular perspective on the putative differences between these two types of synapses (20–22).

Despite the crucial role that inhibitory neurotransmission plays in processing information in the neuronal network, the dynamics of inhibitory synaptic vesicles are poorly understood. In particular, studying the dynamics of single inhibitory synaptic vesicles in hippocampal neurons in real time has been hampered by both technical and practical limitations, including a lack of markers to label individual inhibitory vesicles, the complex three-dimensional structure of inhibitory synapses, and the extremely small size of synaptic vesicles, which have an average diameter of ~40 to 50 nm, well below the resolution of conventional light microscopy (2).

Here, we report the real-time three-dimensional tracking of single GABAergic synaptic vesicles in cultured hippocampal neurons using dual-focus optics and quantum dot (QD)-conjugated antibodies against the luminal domain of the vesicular GABA transporter (VGAT) to selectively label single GABAergic vesicles. We found significant differences between GABAergic synaptic vesicles and Syt1-labeled vesicles with respect to the fusion latency, the total travel length prior to fusion, and the prevalence of kiss-and-run fusion. Moreover, we found that GABAergic synaptic vesicles move more straightly to their release sites than Syt1-labeled vesicles. These findings indicate that inhibitory synaptic vesicles have unique dynamics and fusion properties that support their ability to facilitate rapid neurotransmission.

Results

Real-Time Three-Dimensional Tracking of Single GABAergic Synaptic Vesicles in Cultured Hippocampal Neurons.

To study the dynamics of inhibitory synaptic vesicles in mature synapses, we tracked single GABAergic synaptic vesicles in three dimensions in real time up to the moment of exocytosis in dissociated hippocampal neurons cultured for 14 to 21 days in vitro (DIV) using our previously reported strategy of loading each synaptic vesicle with a single streptavidin-coated QD conjugated to biotinylated antibodies against the luminal domain of endogenous Syt1 (or Syt1-labeled synaptic vesicles); this approach provides with a spatial accuracy on the order of 20 to 30 nm, which is less than the diameter of a synaptic vesicle (23). To specifically load the QDs in GABAergic vesicles, we conjugated streptavidin-coated QDs to commercially available biotinylated antibodies against the luminal domain of the VGAT, as shown in Fig. 1A. Upon exocytosis induced by electrical stimulation, the QD-conjugated antibodies bind to the luminal domain of VGAT, causing the QD to be taken up into the vesicle upon endocytosis. To confirm selective labeling of GABAergic vesicles, we used a CypHer5E-labeled antibodies against the luminal domain of VGAT (VGAT–CypHer5E) (24) to label spontaneously released GABAergic vesicles; this revealed the colocalization between the QD and VGAT–CypHer5E fluorescence signals (Fig. 1B). Only QD-labeled vesicles that were colocalized

with VGAT–CypHer5E were used for studying GABAergic vesicle dynamics and exocytosis.

In our experiments, exocytosis of a QD-loaded vesicle is reflected by a sudden, irreversible drop in QD fluorescence caused by quenching with extracellular Trypan blue (23). To measure the position of single QD-loaded GABAergic synaptic vesicles in the x-y plane, we used fluorescence imaging with one-nanometer accuracy (FIONA) (23, 25, 26); the vesicle's z-position was localized using dual-focus imaging (23, 27). Fig. 1C shows the real-time three-dimensional position of a single QD-loaded GABAergic synaptic vesicle in a cultured neuron stimulated at 10 Hz up to the time of exocytosis; the x-y plane projection is overlaid on the fluorescence image of a GABAergic presynaptic terminal labeled with VGAT–CypHer5E, showing that the GABAergic vesicle remained near the edge of the presynaptic terminal before undergoing exocytosis. Fluorescence images of the QD-loaded GABAergic vesicle just before and after exocytosis show near-complete, irreversible quenching of the QD (Fig. 1D). In addition to measuring the three-dimensional position, we also analyzed the average fluorescence intensity (F) within the region of interest (ROI) and the radial distance (R) between the momentary position and the fusion site using the Pythagorean equation $R = \sqrt{\Delta X^2 + \Delta Y^2 + \Delta Z^2}$ (Fig. 1E). A close examination of the fluorescence trace in Fig. 1E reveals several quantal "photoblinking" events (e.g., at ~8, 13, and 15 s), consistent with the presence of a single QD inside the vesicle lumen, followed by a sharp, irreversible loss of fluorescence at 32 s due to exposure of the QD to the quencher (Trypan blue) in the external solution, indicating exocytosis. This illustrates how the three-dimensional position of a single GABAergic vesicle loaded with a single QD can be tracked in real time up to the moment of exocytosis during electrical stimulation. In all the trajectories reported in this paper, exocytosis occurred after onset of electrical stimulation, not before.

To determine whether QD-conjugated antibodies against the luminal domain of Syt1 label GABAergic synaptic vesicles, we measured the colocalization between VGAT–CypHer5E-labeled GABAergic presynaptic terminals and synaptic vesicles loaded with QD-conjugated antibodies against Syt1. As shown in *SI Appendix*, Fig. S1, we found a relatively low percentage of colocalization between VGAT–CypHer5E terminals and Syt1–QD-loaded vesicles (12 ± 1.4%; n = 13 images), suggesting that our previous measurements of Syt1-labeled vesicles in the hippocampal neurons largely reflect the dynamics of excitatory vesicles (23). In contrast, we found a significantly higher degree of colocalization (61 ± 3.4%; n = 13) between VGAT–CypHer5E-labeled terminals and VGAT–QD-loaded vesicles (*SI Appendix*, Fig. S1 A and C), confirming that VGAT antibody-conjugated QDs label GABAergic synaptic vesicles preferentially.

Next, we examined the relative proportion of inhibitory neurons in our dissociated hippocampal cultures by coimmunostaining the neurons for the neuronal marker microtubule-associated protein 2 (MAP2) and glutamic acid decarboxylase 67 (GAD67), a marker of inhibitory neurons (Fig. 2A). Our analysis revealed 6 ± 0.8% (n = 23 images) colocalization between MAP2$^+$ and GAD67$^+$ cells (Fig. 2B), suggesting that our cultured hippocampal neurons are predominantly comprised of excitatory neurons. Moreover, we found high colocalization (82 ± 7.7%; n = 19) between GAD67 and parvalbumin (PV) immunostaining (Fig. 2C), indicating that the majority of inhibitory neurons in our cultures are PV-expressing fast-spiking GABAergic interneurons. By extension, we conclude that our measurements of VGAT-labeled synaptic vesicles predominantly reflect the dynamics of GABAergic synaptic vesicles in fast-spiking PV-expressing GABAergic interneurons.

GABAergic Synaptic Vesicles Have Unique Spatiotemporal Dynamics.

To understand prefusion dynamics of GABAergic synaptic vesicles, we measured the net displacement between the initial position

www.manaraa.com
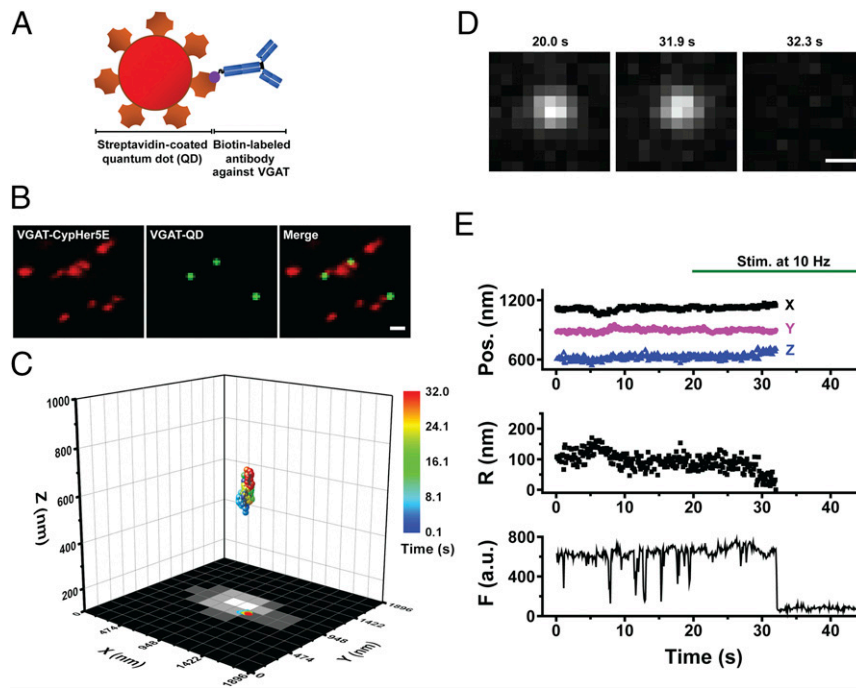
Fig. 1. Real-time three-dimensional tracking of a single GABAergic synaptic vesicle loaded with a single QD. (*A*) Schematic diagram depicting a streptavidin-coated QD conjugated to biotinylated antibodies against the luminal domain of VGAT. (*B*) Colocalization of VGAT–QD-loaded GABAergic synaptic vesicles (green) and VGAT-CypHer5E-labeled presynaptic boutons (red) in cultured hippocampal neurons. (Scale bar, 1 μm.) (*C*) Three-dimensional trajectory of a VGAT–QD-loaded GABAergic vesicle overlaid on the *x-y* plane of a VGAT-CypHer5E-labeled presynaptic bouton. The color bar represents elapsed time; electrical stimulation (10 Hz) started at 20 s, and the vesicle underwent exocytosis at 32.0 s. (*D*) Fluorescence images of the VGAT–QD-loaded vesicle shown in *C* taken at the indicated times. (Scale bar, 0.5 μm.) (*E*) Three-dimensional position, radial distance from the momentary position to the fusion site (R), and fluorescence intensity (F) of the VGAT–QD-loaded vesicle shown in *C*. Note the photoblinking events (e.g., at ~8 s, 13 s, and 15 s), confirming the presence of one QD inside the vesicle. Electrical stimuli (10 Hz) were applied for 120 s starting at 20 s (green horizontal bar).

and the fusion site of individual vesicles while applying electrical stimuli at 10 Hz. The three-dimensional net displacement of each vesicle was calculated as the Pythagorean displacement using our real-time three-dimensional traces of single QD-loaded GABAergic synaptic vesicles. Fig. 3*A* shows the net displacements of GABAergic synaptic vesicles compared with that of our previous data of Syt1-labeled vesicles (23), which used 0.1 nM QD-conjugated antibody to minimize any possible effect by QDs and antibodies (28). The distribution of the net displacement between the initial positions

and fusion sites of GABAergic synaptic vesicles was not significantly different from that of Syt1-labeled synaptic vesicles ($P > 0.7$, Kolmogorov–Smirnov [K-S] test) (Fig. 3*A*).

Next, we measured fusion latency, defined as the interval between the start of stimulation and the moment of fusion. We found that the fusion latency was significantly shorter for GABAergic vesicles (26.2 ± 2.24 s; $n = 80$ vesicles) compared with Syt1-labeled vesicles (44.6 ± 4.89 s; $n = 49$ vesicles) ($P < 0.01$, K-S test) (Fig. 3*B*), indicating that individual inhibitory vesicles
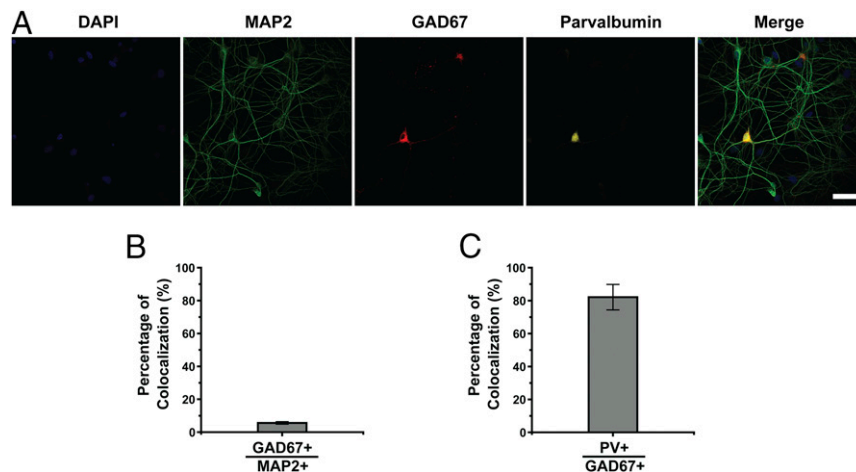
Fig. 2. Inhibitory neurons in hippocampal cultures. (*A*) Representative confocal images of cultured hippocampal neurons immunostained for MAP2 (green), GAD67 (red), and PV (yellow); the nuclei were counterstained with DAPI (blue). (Scale bar, 50 μm.) (*B*) Percentage of GAD67^{+} neurons among all MAP2^{+} neurons. (*C*) Percentage of PV^{+} neurons among all GAD67^{+} neurons. Error bars show SEM.

Park et al.
Unique dynamics and exocytosis properties of GABAergic synaptic vesicles revealed by three-dimensional single vesicle tracking

PNAS | **3 of 10**
https://doi.org/10.1073/pnas.2022133118

NEUROSCIENCE

underwent exocytosis more readily than excitatory vesicles. Within 40 s from the onset of stimulation, 82.5% of GABAergic vesicles (66 of 80 vesicles measured) underwent fusion compared to 53.1% (26 of 49) of Syt1-labeled vesicles, which is consistent with inhibitory vesicles (and nerve terminals) having a higher release probability compared to their excitatory counterparts (17, 18).

To understand why GABAergic vesicles fuse more readily than Syt1-labeled vesicles but have the similar net displacement prior to fusion, we calculated the total three-dimensional travel distance prior to fusion. We found that GABAergic vesicles traveled a significantly shorter distance before undergoing exocytosis compared with Syt1-labeled vesicles (19.2 ± 1.13 μm vs. 27.9 ± 2.47 μm, respectively; $P < 0.05$, K-S test) (Fig. 3C). Taken together, these results indicate that GABAergic vesicles moved to their fusion sites more directly, following a straighter trajectory, compared to Syt1-labeled vesicles, thereby increasing their release probability.

Vesicles must travel to the presynaptic membrane, await a vacancy at the active zone, dock, and establish a preliminary SNARE complex, and then wait for a sufficient Ca^{2+} trigger before undergoing SNARE-mediated fusion. In tracking three-dimensional coordinates, we examined the time taken for the initial steps requiring physical translocation, known as latency to release site. This latency preceded a period of dwelling in close proximity (< 100 nm) to the fusion site, which was defined using a previously described method (23) and is analyzed below (see, for example, Fig. 5I). Of 80 GABAergic synaptic vesicles, 33 had zero latency to release site because of close proximity to their

fusion sites at the onset of stimulation and were excluded from further analysis related to the dynamics before final dwell. Latency to release site was significantly briefer for GABAergic synaptic vesicles (24.8 ± 2.78 s; $n = 47$ vesicles) than Syt1-labeled vesicles (44.9 ± 5.09 s; $n = 35$ vesicles; $P < 0.001$, K-S test) (Fig. 3E). Correspondingly, the total travel length before final dwell was also shorter for GABAergic vesicles than Syt1-labeled vesicles (20.7 ± 1.40 μm vs. 29.1 ± 2.72 μm, respectively; $P < 0.05$, K-S test) (Fig. 3F) though the net displacement before final dwell was not significantly different ($P > 0.1$, K-S test) (Fig. 3D). Thus, GABAergic vesicles are quicker to reach their ultimate fusion sites than their excitatory counterparts, accounting for much of their overall advantage in showing briefer fusion latency.

GABAergic Synaptic Vesicles Move More Straightly to Their Release Sites than Syt1-Labeled Vesicles. We further investigated the motion of GABAergic synaptic vesicles toward their release sites by closer examination of the correlation between latency to release site and motion before final dwell. The net displacement before final dwell was significantly correlated with latency to release site for GABAergic vesicles (Pearson's $r = 0.42$) (Fig. 4A) compared with Syt1-labeled vesicles (Pearson's $r = 0.23$) (Fig. 4B). Moreover, the y-intercept, which describes the time taken to reach the ultimate site of fusion even as global translocation dwindles to zero, was smaller for GABAergic vesicles than Syt1-labeled synaptic vesicles (14.2 ± 4.23 s vs. 37.6 ± 7.46 s, respectively). A possible interpretation is that newly arriving GABAergic vesicles await fusion of their predecessors before docking, but less so than Syt1-labeled vesicles. Using the net displacement before
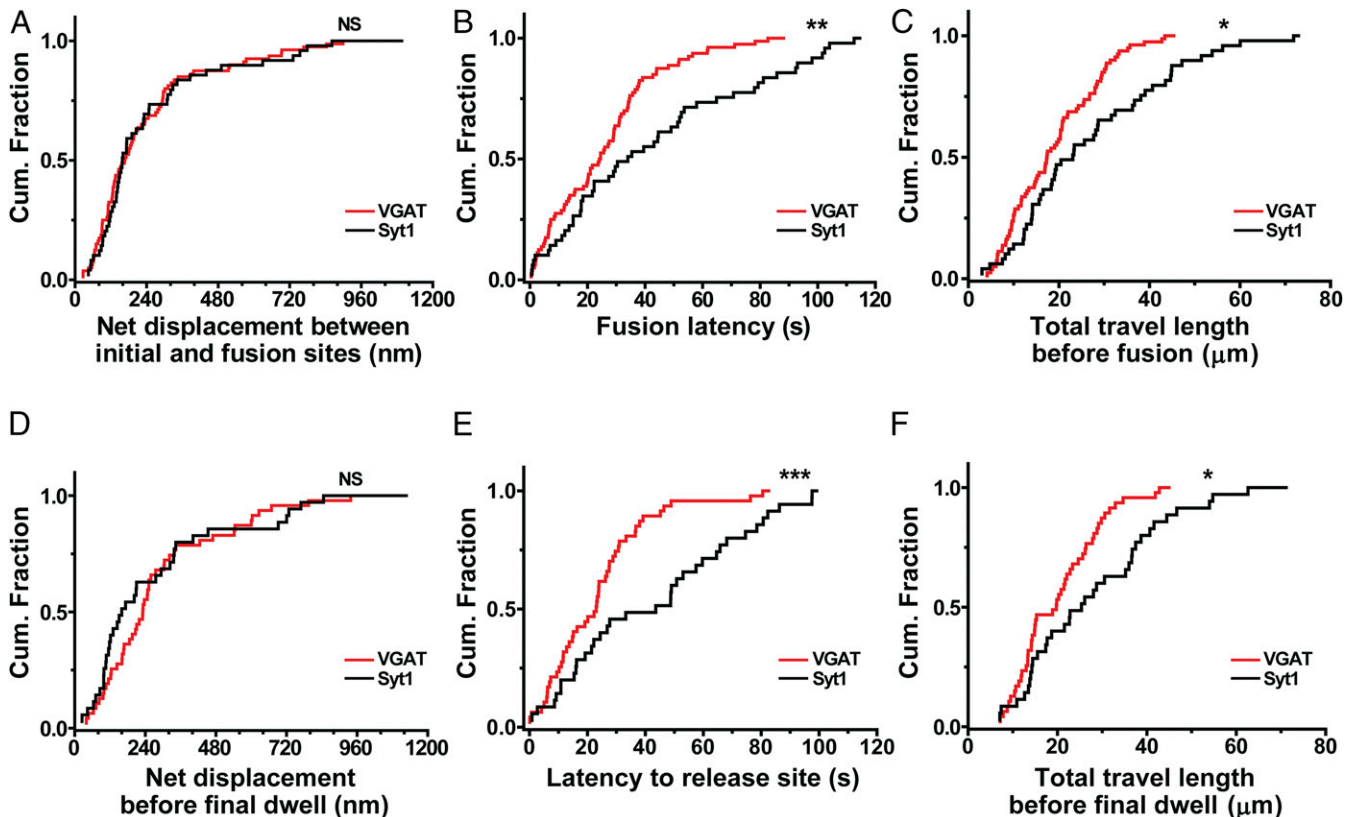
Fig. 3. GABAergic synaptic vesicles have distinct spatiotemporal dynamics. (A–C) Cumulative distribution of the net displacement between initial and fusion sites (A), fusion latency (B), and total travel length before fusion (C) for VGAT–QD-labeled synaptic vesicles (n = 80 vesicles) and Syt1–QD-loaded synaptic vesicles (n = 49 vesicles). (D–F) Cumulative distribution of the net displacement before final dwell (D), latency to release site (E), and total travel length before final dwell (F) for VGAT–QD-labeled synaptic vesicles (n = 47 vesicles) and Syt1–QD-loaded synaptic vesicles (n = 35 vesicles). *P < 0.05, **P < 0.01, ***P < 0.001, and NS, not significant (K-S test).

Park et al.
Unique dynamics and exocytosis properties of GABAergic synaptic vesicles revealed by three-dimensional single vesicle tracking
www.manaraa.com

final dwell, we then calculated the net velocity before final dwell of releasing vesicles. The net velocity before final dwell of GABAergic synaptic vesicles was significantly higher than that of Syt1-labeled vesicles (7.1 ± 0.87 nm/s vs. 5.1 ± 1.12 nm/s, respectively; $P < 0.01$, K-S test) (Fig. 4C), indicating that GABAergic synaptic vesicles move more straightly to their release sites than Syt1-labeled vesicles. The coefficient of variation for the net velocity before final dwell was smaller for GABAergic vesicles (83%) compared to that of Syt1-labeled vesicles (130%), indicating that the net velocity before final dwell of GABAergic vesicles was less variable.

Next, we examined the correlation between latency to release site and the total travel length before final dwell and found a significant correlation for GABAergic vesicles (Pearson's r = 0.79) (Fig. 4D) compared with Syt1-labeled vesicles (Pearson's r = 0.72) (Fig. 4E). Using the total travel length before final dwell, we then calculated the speed before final dwell of releasing GABAergic synaptic vesicles and found that the speed before final dwell of GABAergic synaptic vesicles was similar to that of Syt1-labeled vesicles (464 ± 19.1 nm/s vs. 471 ± 34.8 nm/s, respectively; $P > 0.4$, K-S test) (Fig. 4F), with a smaller coefficient of variation (28% vs. 44%, respectively). Thus, the movement of GABAergic vesicles before final dwell is regulated more tightly compared to Syt1-labeled vesicles, with regard to both speed and direction of motion.

Kiss-and-Run Fusion Is More Prevalent in GABAergic Synaptic Vesicles. Finally, we investigated the exocytotic fusion mode of single inhibitory synaptic vesicles. In kiss-and-run fusion, the fusion pore opens briefly, causing a partial drop in fluorescence due to incomplete quenching by extracellular trypan blue; in contrast, full-collapse fusion causes the near complete loss of fluorescence (23). Fig. 5A shows the fluorescence images of a QD loaded in a GABAergic vesicle undergoing fusion, taken before a drop in fluorescence (70.2 s), after a partial drop in fluorescence (71.2 and 105 s), and after subsequent loss of the remaining fluorescence (105.9 s). The time course of the QD fluorescence—obtained by analyzing an ROI containing the QD—shows a sudden drop in fluorescence at 70.5 s (Fig. 5B, magenta arrow), followed by a further, irreversible drop in fluorescence at 105.2 s (Fig. 5B, blue arrow), representing full-collapse fusion. The fluorescence of the QD for the period after 70.5 s was reduced to 35% of the initial level, larger than the expected level for QDs steadily exposed to 2 μM TB (12%), thus indicating that the GABAergic synaptic vesicle underwent kiss-and-run fusion at 70.5 s.

We then classified all of the fluorescence traces based on their quenching pattern and aligned the traces relative to the drop in
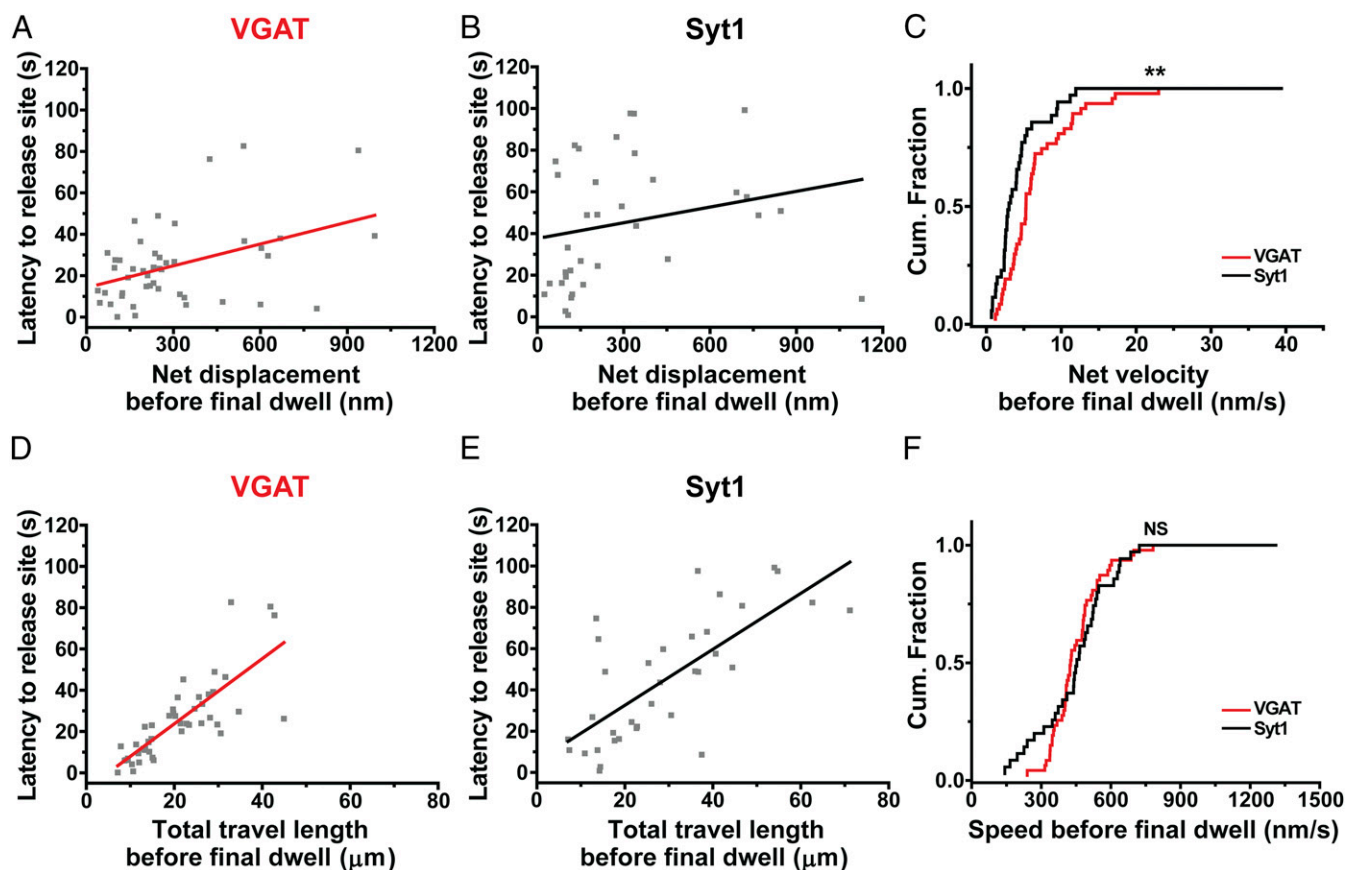
Fig. 4. GABAergic synaptic vesicles move more straightly to their release sites than Syt1-labeled vesicles. (A) Latency to release site of VGAT–QD-labeled synaptic vesicles ($n = 47$ vesicles) is plotted against the net displacement before final dwell. Each symbol represents an individual VGAT–QD-loaded GABAergic vesicle, and the red line represents the linear regression (Pearson's r = 0.42). (B) The relationship between latency to release site and the net displacement before final dwell of Syt1–QD-labeled vesicles ($n = 35$ vesicles). Each symbol represents an individual Syt1–QD-loaded synaptic vesicle. The black line represents the linear regression (Pearson's r = 0.23). (C) Cumulative distribution of net velocity before final dwell measured for VGAT–QD-loaded and Syt1–QD-loaded synaptic vesicles. (D) The relationship between latency to release site and the total travel length before final dwell for VGAT–QD-loaded synaptic vesicles. The red line represents the linear regression (Pearson's r = 0.79). (E) The relationship between latency to release site and the total travel length before final dwell for Syt1–QD-labeled synaptic vesicles. The black line represents the linear regression (Pearson's r = 0.72). (F) Cumulative distribution of speed before final dwell measured for VGAT–QD-loaded and Syt1–QD-loaded synaptic vesicles. **$P < 0.01$ and NS, not significant (K-S test).

Park et al.
Unique dynamics and exocytosis properties of GABAergic synaptic vesicles revealed by three-dimensional single vesicle tracking

PNAS | 5 of 10
https://doi.org/10.1073/pnas.2022133118
www.manaraa.com

NEUROSCIENCE

fluorescence, revealing three patterns: 1) Near-complete loss of fluorescence (presumably representing full-collapse fusion), 2) partial quenching followed by near-complete quenching (presumably representing a kiss-and-run fusion event followed by full-collapse fusion or reuse after the first kiss-and-run fusion event), and 3) partial quenching that was not followed by near-complete quenching (representing a kiss-and-run fusion event that was not followed by full-collapse fusion). These three patterns are shown in Fig. 5 *C1*, *C2*, and *C3*, respectively.

In one pattern (Fig. 5*C1*), the average remaining normalized fluorescence following fusion (0.058 ± 0.0062, $n = 28$) was smaller than 0.12 (the expected normalized fluorescence right after full-collapse fusion), suggesting full-collapse fusion and near-complete quenching; in contrast, the less-complete fluorescence drop in other cases (to 0.226 ± 0.019, $n = 13$ in Fig. 5*C2* and 0.204 ± 0.001, $n = 39$ in Fig. 5*C3*), to levels considerably higher than 0.12, were indicative of kiss-and-run fusion. In the fluorescence traces pooled in Fig. 5*C2*, the initial sharp fluorescence drop was followed by secondary decrease in fluorescence, reflecting reuse of the same vesicle and confirming that the initial drop represented partial quenching.

Using the degree of quenching as a measure of full-collapse fusion versus kiss-and-run fusion, we then measured the prevalence of kiss-and-run fusion in vesicles releasing inhibitory neurotransmitters. We found that approximately two-thirds of GABAergic vesicles that underwent exocytosis exhibited kiss-and-run fusion compared to approximately one-quarter of Syt1-labeled vesicles (Fig. 5*D*), indicating that GABAergic vesicles undergo kiss-and-run fusion more frequently compared with Syt1-labeled vesicles. This relatively high prevalence of kiss-and-run fusion in GABAergic vesicles may contribute to the ability of GABAergic neurons to repeatedly release GABA and thus to preserve inhibitory synaptic strength during prolonged periods of fast spiking of mature GABAergic neurons (18, 29, 30).

We also examined the total travel length and fusion latency of GABAergic synaptic vesicles based on fusion modes and compared them with Syt1-labeled vesicles. We found that among the vesicles that underwent full-collapse fusion, GABAergic vesicles traveled a shorter total distance before fusion compared to Syt1-labeled vesicles (16.9 ± 1.66 μm [$n = 28$] vs. 30.4 ± 3.09 μm [$n = 36$], respectively; $P < 0.05$, K-S test) (Fig. 5*E*). In contrast, when we examined the vesicles that underwent kiss-and-run fusion, we found no significant difference between GABAergic and Syt1-labeled vesicles (20.4 ± 1.48 μm [$n = 52$] vs. 21.0 ± 3.09 μm [$n = 13$], respectively; $P > 0.7$, K-S test) (Fig. 5*F*). Similarly, we found that fusion latency for GABAergic vesicles undergoing full-collapse fusion was significantly shorter than Syt1-labeled vesicles (20.3 ± 3.04 s vs. 44.9 ± 5.84 s, respectively; $P < 0.01$, K-S test) (Fig. 5*G*), but not for vesicles undergoing kiss-and-run fusion (29.5 ± 2.96 s vs. 43.7 ± 9.21 s, respectively; $P > 0.4$, K-S test) (Fig. 5*H*). On the other hand, the net displacement of GABAergic synaptic vesicles was not significantly different compared with Syt1-labeled vesicles regardless of vesicle fusion mode (*SI Appendix*, Fig. S2). Taken together, these results indicate that the unique capability of inhibitory synaptic transmission arises in part from the high prevalence of kiss-and-run fusion (Fig. 5*D*) and in part from the dynamic efficiency of the subgroup of inhibitory vesicles that undergo full-collapse fusion (Fig. 5 *E* and *G*).

Finally, we measured the dwell time at the final position immediately before fusion of GABAergic synaptic vesicles using a previously described method (23). The dwell time immediately before fusion of GABAergic vesicles was not significantly different from that of Syt1-labeled vesicles ($P > 0.3$, K-S test) (Fig. 5*I*), indicating that the observed difference in the dynamics of GABAergic synaptic vesicles and Syt1-labeled vesicles is likely to be caused by their motion to release sites but not by the motion during final dwell. GABAergic synaptic vesicles undergoing kiss-and-run fusion stayed longer at the final position than those undergoing full-collapse fusion (14.0 ± 1.81 s vs. 7.4 ± 1.35 s, respectively; $P < 0.05$, K-S test) (Fig. 5*J*), similar to the pattern found for Syt1-labeled vesicles (23). Taken together, these results support the notion that inhibitory synaptic vesicles have unique dynamics and exocytosis properties compared with excitatory vesicles.

Discussion

GABAergic inhibitory synapses differ from glutamatergic excitatory synapses with respect to both structure and function. In the central nervous system, GABAergic neurons play a critical role in controlling the activity of glutamatergic neurons via rapid feedforward and feedback inhibitory mechanisms (18, 31, 32). The demands on transmission are quantitatively greater for inhibitory neurons than excitatory neurons, arising from higher rates of spike firing, estimated as 5- to 10-fold faster in vivo (33). To allow for rapid synaptic transmission with high fidelity, inhibitory neurons have a distinct set of properties, including morphology, multiplicity of release sites, biogenesis, and trafficking of synaptic vesicles in the presynaptic terminal (21, 34–36). Importantly, the release machinery at GABAergic synapses is tightly coupled to voltage-gated Ca^{2+} channels, thereby maximizing the speed and efficacy of GABAergic transmission (37, 38). While the relatively high release probability and fidelity of action potential-evoked Ca^{2+} signaling clearly play an important role in maintaining temporally precise GABAergic transmission, the mode of exocytosis and dynamics of single GABAergic vesicles have not been investigated due to technical limitations.

Here, we selectively loaded GABAergic synaptic vesicles in hippocampal neurons with QDs conjugated to antibodies against the luminal domain of VGAT and then tracked their three-dimensional position in real time up to the moment of exocytosis. We then compared these dynamics with synaptic vesicles labeled with QDs conjugated to antibodies against the luminal domain of Syt1. Although Syt1 serves as the putative Ca^{2+} sensor in both glutamatergic and GABAergic presynaptic terminals (39), the great majority of the Syt1-labeled vesicles appeared to be excitatory; only ~10% colocalized with VGAT–CypHer5E-labeled presynaptic terminals. Thus, our previous data obtained using Syt1-labeled synaptic vesicles in cultured hippocampal neurons (23) likely report dynamics of excitatory vesicles, although they may also reflect a small number of inhibitory vesicles. Even though the hippocampus contains more than 21 subtypes of interneurons (8), our immunostaining results indicate that ~80% of the inhibitory neurons in our hippocampal cultures express PV. This supports use of data obtained from synaptic vesicles labeled via Syt1 (23) and VGAT as a first approximation to comparing vesicle dynamics within excitatory boutons and PV[+] inhibitory boutons. Any contribution of GABAergic vesicles to those labeled via Syt1 would render our results as underestimates of distinctions between excitatory and inhibitory vesicles.

By focusing on the unitary properties of single inhibitory vesicles, our optical experiments provide perspective complementary to recordings of GABAergic neurotransmission. A QD-labeled vesicle, having undergone QD uptake via clathrin-mediated retrieval (40), must start off as initially unavailable for fusion. The labeled vesicles can then travel to the release site, prepare for fusion, and eventually fuse sometime during the period of repetitive stimulation. The first part of this progression in status, the transition from unavailable to releasable, was depicted as a simple first-order transition in a model of PV[+] presynaptic vesicular pools based on electrophysiological data (18). The fitted unidirectional rate, $k' = 0.059$/s, is comparable to vesicular dynamics we observed in optical recordings (Fig. 3*B*). Thus, monitoring the motion of GABAergic vesicles offers direct insight into a crucial kinetic step at the single vesicle level.
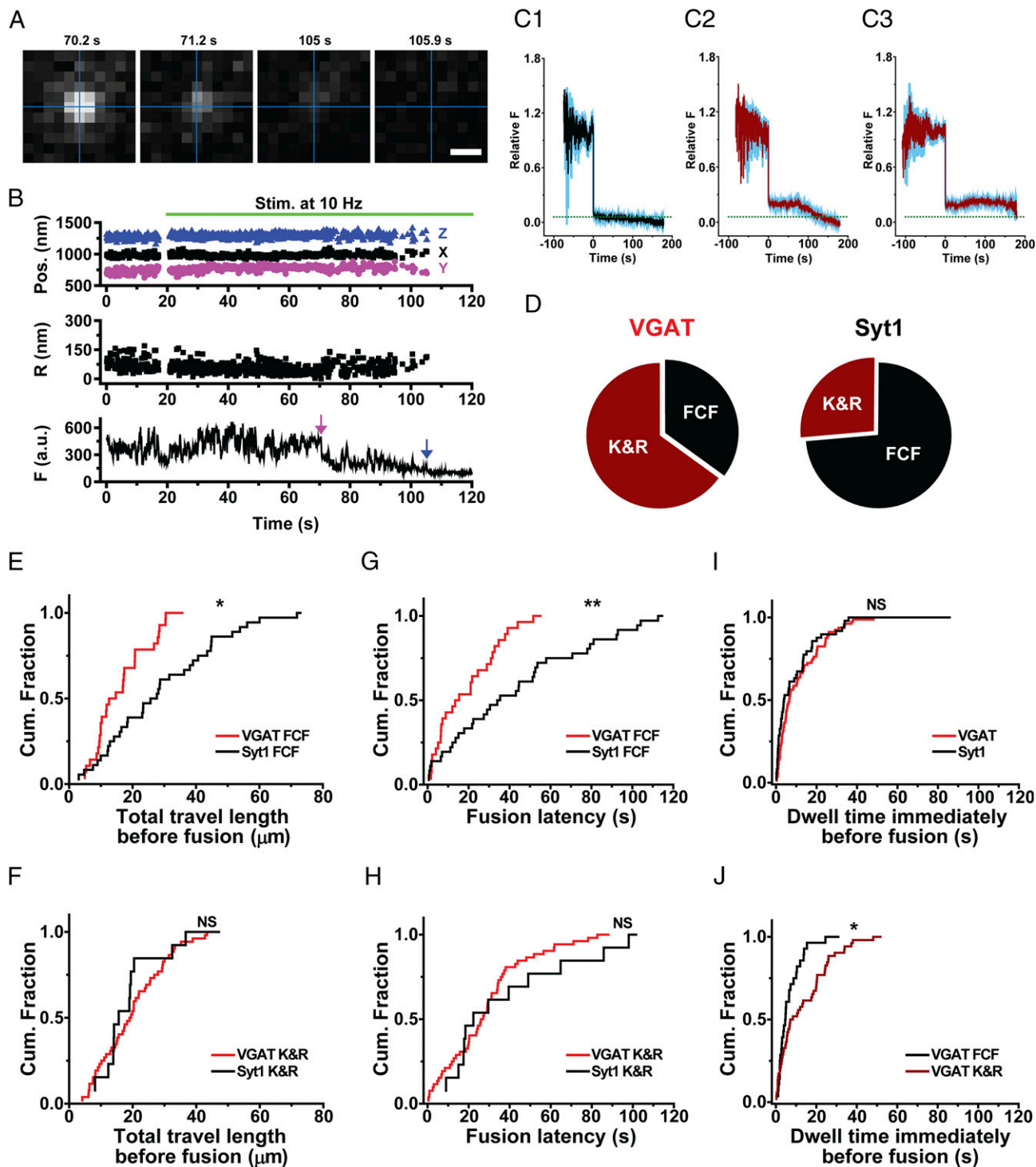
Fig. 5. Exocytotic fusion mode of GABAergic synaptic vesicles. (*A*) Fluorescence images taken at the indicated times for a GABAergic synaptic vesicle loaded with a VGAT-conjugated QD; electrical stimuli (10 Hz) were applied at 20 s. The intersection of the perpendicular lines marked the position of the vesicle before the first fusion. (Scale bar, 0.5 μm.) (*B*) Three-dimensional position, radial distance (R), and fluorescence (F) of a VGAT–QD-loaded vesicle that underwent kiss-and-run (K&R) fusion (magenta arrow) followed by full-collapse fusion (FCF, blue arrow). Electrical stimuli (10 Hz) were applied for 120 s starting at 20 s (green horizontal bar). (*C*) Average normalized fluorescence intensity traces (with SEM) time-aligned to the first fusion event for vesicles that underwent FCF (*C1*), vesicles that underwent K&R fusion followed by FCF (*C2*), and vesicles that underwent K&R fusion but never underwent FCF (*C3*). The dotted horizontal line represents an average normalized fluorescence intensity value after FCF (0.058). (*D*) Relative distribution of the fusion modes measured in VGAT–QD-loaded and Syt1–QD-loaded vesicles that underwent exocytosis; 65% and 27% of vesicles, respectively, underwent K&R fusion. (*E* and *F*) Cumulative distribution of total travel length for VGAT–QD-loaded and Syt1–QD-loaded vesicles that underwent either FCF (*E*) or K&R fusion (*F*). (*G* and *H*) Cumulative distribution of fusion latency for VGAT–QD-loaded and Syt1–QD-loaded vesicles that underwent either FCF (*G*) or K&R fusion (*H*). (*I*) Cumulative distribution of the dwell time at the final position immediately before fusion for VGAT–QD-loaded (VGAT) and Syt1–QD-loaded (Syt1) synaptic vesicles. (*J*) Cumulative distribution of the dwell time immediately before fusion for VGAT–QD-loaded vesicles that underwent either FCF (VGAT FCF) or K&R fusion (VGAT K&R). *$P < 0.05$, **$P < 0.01$, and NS, not significant (K-S test).

Park et al.
Unique dynamics and exocytosis properties of GABAergic synaptic vesicles revealed by three-dimensional single vesicle tracking

PNAS | 7 of 10
https://doi.org/10.1073/pnas.2022133118

Overall, we found that the total travel length traversed by GABAergic vesicles was smaller compared with Syt1-labeled vesicles. We also found that GABAergic vesicles underwent exocytosis earlier than Syt1-labeled vesicles, with a larger percentage of GABAergic vesicles undergoing release within 40 s after the onset of stimulation. These results indicate that GABAergic synaptic vesicles travel to their fusion sites by following a more direct route compared to Syt1-labeled vesicles, contributing to their higher release probability. Interestingly, we also found that kiss-and-run fusion is more prevalent among GABAergic vesicles compared with Syt1-labeled vesicles. Taken together, these differences between GABAergic and Syt1-labeled vesicles indicate that GABAergic vesicles have a distinct set of dynamics and exocytosis properties, consistent with previous reports that GABAergic synapses have unique electrophysiological and ultrastructural features, including a larger RRP, higher vesicle release probability, and ability to resist complete loss of synaptic strength because of vesicle depletion (17, 18, 29, 30).

These properties of single GABAergic synaptic vesicles support the efficient and rapid release of neurotransmitters from PV-expressing inhibitory neurons, enabling increased microcircuit functions in the brain, including feedforward and feedback inhibition as well as high-frequency network oscillations on a rapid time scale (41). The differences between GABAergic and Syt1-labeled vesicles with respect to their release dynamics suggest that differences in these vesicles affect synaptic function, despite having (at least partially) similar molecular release machinery. Consistent with the importance of vesicle localization and movement, alteration in the location and dynamics of synaptic vesicles may perturb the release of neurotransmitters in neurodegenerative diseases (42, 43).

The unique dynamics of single inhibitory synaptic vesicles likely contribute to rapid inhibitory neurotransmission. Specifically, their shorter travel length prior to exocytosis and high release probability enable inhibitory vesicles to undergo exocytosis earlier and with higher fidelity compared to excitatory vesicles, which is reflected by their significantly shorter time to fusion. In addition, other mechanisms may also contribute to rapid inhibitory neurotransmission. Although the precise mechanism underlying the unique dynamics associated with inhibitory vesicles is currently unknown, several possibilities come to mind, including distinct types of intervesicular links (44) or different modes of motion shown in ensemble measurement of synaptic vesicles (45, 46). Whatever the mechanism, it is noteworthy that inhibitory vesicles that fuse by full-collapse fusion do so quickly, enhancing the dynamic capability of the inhibitory boutons. On the other hand, we also observed that inhibitory boutons marshal their vesicular resources in multiple ways. First, a significant fraction of vesicles appears unavailable to undergo fusion during a single bout of stimulation (*SI Appendix*, Fig. S3), as if they were sequestered in an unavailable pool to enhance the durability of inhibitory transmission (18). Second, some of GABAergic synaptic vesicles that undergo kiss-and-run fusion (manifested as a partial degree of QD quenching) also support vesicular reuse (reflected by a delayed secondary drop in QD fluorescence) (Fig. 5C2), another form of vesicular economy. Third, other QDs fuse, but retain their identity throughout the rest of the stimulation (Fig. 5C3), thereby remaining available for recruitment in a later round of activity. Thus, the capability of rapid, immediate vesicle release seems to be counterbalanced in multiple ways by features that safeguard vesicular resources for future deployment, as predicted by Kraushaar and Jonas (18). Taken together, these data show that vesicle dynamics help support rapid inhibitory neurotransmission on the one hand, while tuning the degree of synaptic fatigue on the other (9, 18).

The molecular mechanism underlying the observed distinct features of GABAergic synaptic vesicles remains to be determined. Vesicles must first travel to the vicinity of the final fusion site, await vacancies at the active zone, then dock and undergo preparation of their SNARE machinery (1, 4). Our observations indicate that GABAergic vesicles are quicker than Syt1 vesicles to arrive near the release site (Fig. 3E), accounting for much of the difference in fusion latency (Fig. 3B). Other possible distinctions may contribute subsequently to such arrival. Syt2, the main Ca^{2+} sensor of exocytosis in central inhibitory neurons (47), can generate the fastest time course of neurotransmitter release (48, 49), have a tight coupling with Ca^{2+} channels for exocytosis (38), and mediate faster refilling of synaptic vesicles pools (47). Another possible factor is that GABAergic neurons initiate exocytosis through selective use of P/Q-type voltage-gated Ca^{2+} channels (50), which contribute to fast neurotransmitter release through rapid activation and high efficacy (51). Another possible mechanism is that different synapsins are involved in GABAergic synaptic vesicles compared with excitatory synaptic vesicles (20–22). Thus, the detailed molecular mechanism for distinct properties of GABAergic synaptic vesicles warrants further research. The observed shorter fusion latency of GABAergic synaptic vesicles along with rapid responses of ionotropic GABA receptors allows faster inhibitory synaptic transmission in the brain, which plays a crucial role in fast feedforward and feedback inhibition (18, 31, 32, 52) and γ-oscillations (7, 53, 54). Our findings were obtained from in vitro primary hippocampal neurons and need to be tested in vivo because cultured primary neurons lack the full pattern of interactions with other neurons and other types of cells in the neuronal network and might be in different environment from the brain.

In summary, we provide direct evidence that inhibitory vesicles in cultured hippocampal neurons reach their fusion site more directly and quickly, undergo exocytosis earlier, and have a higher prevalence of kiss-and-run fusion compared to Syt1-labeled vesicles. These unique properties may help explain the highly precise manner in which input signals are converted to output signals in inhibitory neurons, providing new insights into how inhibitory neurotransmission contributes to coordination between excitation and inhibition in the central nervous system.

Materials and Methods

Primary Hippocampal Neuron Culture. Rat (Sprague–Dawley) pups at the postnatal 0-day (P0) were killed to harvest CA1 and CA3 of the hippocampal regions of the brain tissue, as previously described (23, 55). All procedures were performed according to the animal protocol approved by the Department of Health, Government of Hong Kong. Around 2×10^4 neurons were plated on each Poly D-Lysine (P7886, Sigma-Aldrich)-coated cover glass with a diameter of 12 mm (Glaswarenfabrik Karl Hecht) in 24-well plates. Two days after plating the neurons, 10 μM uridine (U3003, Sigma-Aldrich) and 10 μM 5-fluorodeoxyuridine (F0503, Sigma-Aldrich) were added to inhibit the proliferation of glial cells in cultured neurons (56). The neurons were cultured in the Neurobasal-A Medium (10888022, Thermo Fisher Scientific) supplemented with 2.5% FBS, 1% penicillin-streptomycin (15140122, Thermo Fisher Scientific), 500 μM GlutaMAX-I Supplement (A1286001, Thermo Fisher Scientific), and 2% B-27 Supplement (17504001, Thermo Fisher Scientific). Cultured neurons were maintained in a 5% CO_2 incubator at 37 °C before experiments were performed.

Microscopy Set-Up. A real-time three-dimensional tracking microscope with a custom-built dual-focus imaging optics was built as previously described (23). The dual-focus imaging optics was made up of an aperture, a beam splitter, lenses, mirrors, and a right-angle mirror. In the dual-focus imaging optics, the beam splitter divided fluorescent signals into two beam pathways, the focus plane of each beam pathway was determined by its lens, and two fluorescence signals from each beam pathway were imaged side-by-side in an electron multiplying (EM) CCD camera. An Olympus IX-73 inverted fluorescence microscope (Olympus) equipped with an EMCCD camera (iXon Ultra, Andor, UK) was used to acquire fluorescence signals, as previously described (57). An oil immersion 100× objective with NA = 1.40 (UPlanSAPO, Olympus) was used for imaging Streptavidin-coated QD (QD 625, A10196, Life Technologies)-conjugated antibodies against VGAT and CypHer5E-conjugated antibodies against VGAT. In order to locate two-dimensional centroids and to calculate the fluorescent peak intensity at different focal

planes (I_1 and I_2), we used custom-written IDL-coded programs (L3Harris Geospatial) to fit a two-dimensional Gaussian function to the fluorescence image. An objective scanner (P-725.2CD, Physik Instrumente) was used to generate a calibration curve based on the *z*-position dependence of the normalized intensity difference $[(I_1 - I_2)/(I_1 + I_2)]$. Custom-made programs written in LabVIEW (National Instruments) were used to control an objective scanner and acquire data on the *z*-position. The *z*-positions of QDs were obtained from the relative peak intensity differences using the empirically determined calibration curve, as previously described (23, 27). A 405-nm laser (OBIS, Coherent Inc.) and a 640-nm laser (OBIS, Coherent Inc.) were used to illuminate streptavidin-coated QDs and CypHer5E, respectively. A 15× beam expander (Edmund Optics) and a focus lens (Newport Corporation) were used to illuminate the sample uniformly.

Real-Time Imaging of Single GABAergic Synaptic Vesicles. Imaging experiments were performed using rat primary hippocampal neurons at 14 to 21 days in vitro at room temperature. Neurons were preincubated with 3 nM of CypHer5E-tagged anti-VGAT antibodies (131 103 CpH, Synaptic Systems) in the culture medium and incubated in the 5% CO_2 incubator for 2 h at 37 °C to specifically label spontaneously recycling GABAergic synaptic vesicles in presynaptic terminals. Then, single GABAergic synaptic vesicles were labeled by QDs conjugated with antibodies against the luminal domain of VGAT. To conjugate QDs to antibodies, streptavidin-coated QD 625 (A10196, Thermo Fisher Scientific) were incubated with biotinylated antibodies against the luminal domain of VGAT (131 103BT, Synaptic Systems) in a modified Tyrode's solution (4 mM KCl, 150 mM NaCl, 2 mM $CaCl_2$, 2 mM $MgCl_2$, 10 mM D-glucose, 10 mM HEPES, 310 to 315 mOsm/kg, and pH 7.3 to 7.4) with casein (C7078, Sigma-Aldrich) for 50 min at room temperature. After the incubation, around 0.4 nM antibody-conjugated QD was added to a sample chamber containing a cover glass with neurons dipped in the modified Tyrode's solution to label one QD per bouton and to minimize any possible effect of antibodies against the luminal domains on normal synaptic transmission. The labeling of single GABAergic synaptic vesicles with QDs was conducted by triggering evoked release of synaptic vesicles using a 10-Hz electric field stimulation for 120 s, which was induced by parallel platinum electrodes connected with the SD9 Grass stimulator (Grass Instruments). Following 2-min incubation after stimulation, the Tyrode's solution was superfused for 15 min at 1.0 ~ 2.0 mL/min. Subsequently, 2 μM of Trypan blue (15250061, Thermo Fisher Scientific) were superfused before imaging. During the imaging, Trypan blue (quencher) was kept in the chamber to quench the fluorescence of QDs exposed to the external solution during exocytosis. Fluorescence images of CypHer5E-labeled and QD-labeled synaptic vesicles were acquired using an Olympus IX-73 inverted microscope. A ZT640rdc-UF1 (Chroma Technology) and an ET690/50M (Chroma Technology) were used to acquire fluorescence images of CypHer5E-labeled presynaptic boutons. A ZT405rdc-UF1 (Chroma Technology) and an ET605/70M (Chroma Technology) were used to acquire fluorescence images of QD-labeled GABAergic synaptic vesicles. Next, 2,000 frame images were obtained using a frame-transfer mode at 10 Hz for 200 s using an EMCCD camera. The EMCCD camera and the stimulator were synchronized with Axon Digidata 1550 (Molecular Devices) to trigger an electric field stimulation at 10 Hz for 120 s while recording. Clampex (program, Molecular Devices) was used to generate stimulation protocols and control stimulation based on the protocol.

Analysis of the Real-Time Single Vesicle Tracking Images. Custom-written IDL-coded programs were used to localize the centroids of raw fluorescence images. Two-dimensional centroids and peak intensities of synaptic vesicles loaded with QDs at two different focal planes were calculated by fitting a Gaussian function to fluorescence images using custom-written programs using IDL. The position along the *z* axis was calculated based on a calibration curve while the average intensity of the fluorescence of a QD within an ROI was calculated using MetaMorph (Molecular Devices). Fusion positions and times of single synaptic vesicles were determined as the first quenching positions and times of fluorescence intensity by Trypan blue during electrical stimulation similar to the previous report (23). The net displacement of a releasing vesicle was calculated as the Pythagorean displacement between the position at the start of imaging and its fusion site. The total travel length was calculated as the total traveling distance between the start of imaging and the point of fusion. The fusion latency was defined as the interval between the start of stimulation and the moment of fusion. The final dwell time was defined as time of terminal residency less than 100 nm away from its fusion site under electrical stimuli (23). The latency to release site was defined as the interval between the start of stimulation and the beginning of final dwell, and was chosen as a conservative estimate of the travel time to the release site of a releasing vesicle. The net displacement before final dwell was calculated as the Pythagorean displacement between the position at the start of imaging and its position at the beginning of final dwell. The total travel length before final dwell was calculated as the total traveling distance between the start of imaging and the beginning of final dwell. Two-sample K-S tests were used for statistical analysis, using OriginPro 9.1 (OriginLab). Data are presented as the mean ± SEM. Differences with $P < 0.05$ were considered significant.

Immunofluorescence. For immunocytochemistry, neurons at DIV 14 were washed with PBS once, then fixed with ice-cold 100% methanol for 10 min at −20 °C. After three washes in PBS for 30 min at room temperature, cells were incubated with chicken polyclonal antibodies against MAP2 (1:1,000; ab5392, Abcam), rabbit polyclonal antibodies against PV (1:500; PA1-933, Thermo Fischer Scientific), and mouse monoclonal antibodies against GAD67 (1:500; MAB5406, Sigma-Aldrich) in staining buffer (0.2% BSA, 0.8 M NaCl, 0.5% Triton X-100, 30 mM phosphate buffer, pH 7.4) overnight at 4 °C. Neurons were then washed three times in PBS for 30 min at room temperature and incubated with Alexa Fluor conjugated secondary antibodies (goat anti-chicken-Alexa 488, A11039; goat anti-rabbit Alexa 568, A11011; donkey anti-mouse Alexa 647, A31571, Life Technologies) with 1:1,000 dilution in staining buffer for 2 h at room temperature and stained with DAPI (300 nM, D1306, Thermo Fisher Scientific) for 10 min at room temperature. After being washed three times in PBS for 30 min, cover glasses were mounted onto microscope slides with HydroMount medium (National Diagnostics). Confocal images were acquired using a SP8 confocal microscope (Leica) with a 40× oil objective.

Quantification of Colocalization. The biotinylated mouse monoclonal anti-Syt1 antibodies (105 311BT, Synaptic Systems) or the biotinylated rabbit polyclonal anti-VGAT antibodies (131 103BT, Synaptic Systems) were conjugated to streptavidin-coated QDs (cat. A10196, Thermo Fisher Scientific), and vesicles were loaded as described previously (23). The rabbit polyclonal anti-VGAT antibodies conjugated to CypHer5E (cat. 131 103CpH, Synaptic Systems) were used to label GABAergic presynaptic terminals by incubation for 3 h. Syt1-QD-loaded or VGAT-QD-loaded vesicles localized to VGAT–CypHer5E-labeled presynaptic boutons were manually counted based on colocalization between the QD and CypHer5E fluorescence signals.

Data Availability. Excel files containing information on three-dimensional tracking of quantum dots labeling synaptic vesicles have been deposited in the New York University Data Catalog (https://datacatalog.med.nyu.edu/dataset/10426) (58).

1. T. C. Südhof, Calcium control of neurotransmitter release. *Cold Spring Harb. Perspect. Biol.* **4**, a011353 (2012).
2. C. Yu, M. Zhang, X. Qin, X. Yang, H. Park, Real-time imaging of single synaptic vesicles in live neurons. *Front. Biol.* **11**, 109–118 (2016).
3. V. N. Murthy, P. De Camilli, Cell biology of the presynaptic terminal. *Annu. Rev. Neurosci.* **26**, 701–728 (2003).
4. T. C. Südhof, Neurotransmitter release: The last millisecond in the life of a synaptic vesicle. *Neuron* **80**, 675–690 (2013).
5. A. Malgaroli, R. W. Tsien, Glutamate-induced long-term potentiation of the frequency of miniature synaptic currents in cultured hippocampal neurons. *Nature* **357**, 134–139 (1992).
6. S. Kim *et al.*, Loss of IQSEC3 disrupts GABAergic synapse maintenance and decreases somatostatin expression in the Hippocampus. *Cell Rep.* **30**, 1995–2005.e5 (2020).
7. G. Buzsáki, *Rhythms of the Brain* (Oxford University Press, 2011).
8. T. Klausberger, P. Somogyi, Neuronal diversity and temporal dynamics: The unity of hippocampal circuit operations. *Science* **321**, 53–57 (2008).
9. S. F. Owen *et al.*, Oxytocin enhances hippocampal spike transmission by modulating fast-spiking interneurons. *Nature* **500**, 458–462 (2013).
10. H. L. Atwood, S. Karunanithi, Diversification of synaptic strength: Presynaptic elements. *Nat. Rev. Neurosci.* **3**, 497–516 (2002).

Park et al.
Unique dynamics and exocytosis properties of GABAergic synaptic vesicles revealed by three-dimensional single vesicle tracking

PNAS | 9 of 10
https://doi.org/10.1073/pnas.2022133118

www.manaraa.com

11. P. S. Kaeser, W. G. Regehr, The readily releasable pool of synaptic vesicles. *Curr. Opin. Neurobiol.* **43**, 63–70 (2017).

12. M. Kneussel, T. J. Hausrat, Postsynaptic neurotransmitter receptor reserve pools for synaptic potentiation. *Trends Neurosci.* **39**, 170–182 (2016).

13. M. Yoshihara, J. T. Littleton, Synaptotagmin I functions as a calcium sensor to synchronize neurotransmitter release. *Neuron* **36**, 897–908 (2002).

14. O. D. Bello *et al.*, Synaptotagmin oligomerization is essential for calcium control of regulated exocytosis. *Proc. Natl. Acad. Sci. U.S.A.* **115**, E7624–E7631 (2018).

15. K. Grushin *et al.*, Structural basis for the clamping and Ca²⁺ activation of SNARE-mediated fusion by synaptotagmin. *Nat. Commun.* **10**, 2413 (2019).

16. G. Voglis, N. Tavernarakis, The role of synaptic ion channels in synaptic plasticity. *EMBO Rep.* **7**, 1104–1110 (2006).

17. R. Nair *et al.*, Neurobeachin regulates neurotransmitter receptor trafficking to synapses. *J. Cell Biol.* **200**, 61–80 (2013).

18. U. Kraushaar, P. Jonas, Efficacy and stability of quantal GABA release at a hippocampal interneuron-principal neuron synapse. *J. Neurosci.* **20**, 5594–5607 (2000).

19. K. Jensen, J. D. Lambert, M. S. Jensen, Activity-dependent depression of GABAergic IPSCs in cultured hippocampal neurons. *J. Neurophysiol.* **82**, 42–49 (1999).

20. S. H. Song, G. J. Augustine, Synapsin isoforms regulating GABA release from hippocampal interneurons. *J. Neurosci.* **36**, 6742–6757 (2016).

21. D. Gitler *et al.*, Different presynaptic roles of synapsins at excitatory and inhibitory synapses. *J. Neurosci.* **24**, 11368–11380 (2004).

22. S. Terada, T. Tsujimoto, Y. Takei, T. Takahashi, N. Hirokawa, Impairment of inhibitory synaptic transmission in mice lacking synapsin I. *J. Cell Biol.* **145**, 1039–1048 (1999).

23. H. Park, Y. Li, R. W. Tsien, Influence of synaptic vesicle position on release probability and exocytotic fusion mode. *Science* **335**, 1362–1366 (2012).

24. Y. Hua *et al.*, A readily retrievable pool of synaptic vesicles. *Nat. Neurosci.* **14**, 833–839 (2011).

25. H. Park, E. Toprak, P. R. Selvin, Single-molecule fluorescence to study molecular motors. *Q. Rev. Biophys.* **40**, 87–111 (2007).

26. A. Yildiz, P. R. Selvin, Fluorescence imaging with one nanometer accuracy: Application to molecular motors. *Acc. Chem. Res.* **38**, 574–582 (2005).

27. T. M. Watanabe, T. Sato, K. Gonda, H. Higuchi, Three-dimensional nanometry of vesicle transport in living cells using dual-focus imaging optics. *Biochem. Biophys. Res. Commun.* **359**, 1–7 (2007).

28. O. A. Afuwape, C. R. Wasser, T. Schikorski, E. T. Kavalali, Synaptic vesicle pool-specific modification of neurotransmitter release by intravesicular free radical generation. *J. Physiol.* **595**, 1223–1238 (2017).

29. M. Galarreta, S. Hestrin, Frequency-dependent synaptic depression and the balance of excitation and inhibition in the neocortex. *Nat. Neurosci.* **1**, 587–594 (1998).

30. J. A. Varela, S. Song, G. G. Turrigiano, S. B. Nelson, Differential depression at excitatory and inhibitory synapses in visual cortex. *J. Neurosci.* **19**, 4293–4304 (1999).

31. Y. Chagnac-Amitai, B. W. Connors, Horizontal spread of synchronized activity in neocortex and its control by GABA-mediated inhibition. *J. Neurophysiol.* **61**, 747–758 (1989).

32. F. Manseau *et al.*, Desynchronization of neocortical networks by asynchronous release of GABA at autaptic and synaptic contacts from fast-spiking interneurons. *PLoS Biol.* **8**, e1000492 (2010).

33. S. M. Cohen *et al.*, Excitation-transcription coupling in parvalbumin-positive interneurons employs a novel CaM kinase-dependent pathway distinct from excitatory neurons. *Neuron* **90**, 292–307 (2016).

34. B. High, A. A. Cole, X. Chen, T. S. Reese, Electron microscopic tomography reveals discrete transcleft elements at excitatory and inhibitory synapses. *Front. Synaptic Neurosci.* **7**, 9 (2015).

35. C. L. Tao *et al.*, Differentiation and characterization of excitatory and inhibitory synapses by cryo-electron tomography and correlative microscopy. *J. Neurosci.* **38**, 1493–1510 (2018).

36. X. Li *et al.*, Presynaptic endosomal cathepsin D regulates the biogenesis of GABAergic synaptic vesicles. *Cell Rep.* **28**, 1015–1028.e5 (2019).

37. C. Williams *et al.*, Coactivation of multiple tightly coupled calcium channels triggers spontaneous release of GABA. *Nat. Neurosci.* **15**, 1195–1197 (2012).

38. I. Bucurenciu, A. Kulik, B. Schwaller, M. Frotscher, P. Jonas, Nanodomain coupling between Ca2+ channels and Ca2+ sensors promotes fast and efficient transmitter release at a cortical GABAergic synapse. *Neuron* **57**, 536–545 (2008).

39. N. A. Courtney, J. S. Briguglio, M. M. Bradberry, C. Greer, E. R. Chapman, Excitatory and inhibitory neurons utilize different Ca²⁺ sensors and sources to regulate spontaneous release. *Neuron* **98**, 977–991.e5 (2018).

40. Q. Zhang, Y.-Q. Cao, R. W. Tsien, Quantum dots provide an optical signal specific to full collapse fusion of synaptic vesicles. *Proc. Natl. Acad. Sci. U.S.A.* **104**, 17843–17848 (2007).

41. H. Hu, F. C. Roth, D. Vandael, P. Jonas, Complementary tuning of Na⁺ and K⁺ channel gating underlies fast and energy-efficient action potentials in GABAergic interneuron axons. *Neuron* **98**, 156–165.e6 (2018).

42. S. T. Brady, G. A. Morfini, Regulation of motor proteins, axonal transport deficits and adult-onset neurodegenerative diseases. *Neurobiol. Dis.* **105**, 273–282 (2017).

43. S. Chen *et al.*, Altered synaptic vesicle release and Ca²⁺ influx at single presynaptic terminals of cortical neurons in a knock-in mouse model of Huntington's disease. *Front. Mol. Neurosci.* **11**, 478 (2018).

44. A. A. Alabi, R. W. Tsien, Perspectives on kiss-and-run: Role in exocytosis, endocytosis, and neurotransmission. *Annu. Rev. Physiol.* **75**, 393–422 (2013).

45. D. Kamin *et al.*, High- and low-mobility stages in the synaptic vesicle cycle. *Biophys. J.* **99**, 675–684 (2010).

46. R. Jordan, E. A. Lemke, J. Klingauf, Visualization of synaptic vesicle movement in intact synaptic boutons using fluorescence fluctuation spectroscopy. *Biophys. J.* **89**, 2091–2102 (2005).

47. C. Chen, I. Arai, R. Satterfield, S. M. Young Jr, P. Jonas, Synaptotagmin 2 is the fast Ca²⁺ sensor at a central inhibitory synapse. *Cell Rep.* **18**, 723–736 (2017).

48. J. Xu, T. Mashimo, T. C. Südhof, Synaptotagmin-1, -2, and -9: Ca(2+) sensors for fast release that specify distinct presynaptic properties in subsets of neurons. *Neuron* **54**, 567–581 (2007).

49. A. M. Kerr, E. Reisinger, P. Jonas, Differential dependence of phasic transmitter release on synaptotagmin 1 at GABAergic and glutamatergic hippocampal synapses. *Proc. Natl. Acad. Sci. U.S.A.* **105**, 15581–15586 (2008).

50. A. V. Zaitsev, N. V. Povysheva, D. A. Lewis, L. S. Krimer, P/Q-type, but not N-type, calcium channels mediate GABA release from fast-spiking interneurons to pyramidal cells in rat prefrontal cortex. *J. Neurophysiol.* **97**, 3567–3573 (2007).

51. L. Li, J. Bischofberger, P. Jonas, Differential gating and recruitment of P/Q-, N-, and R-type Ca2+ channels in hippocampal mossy fiber boutons. *J. Neurosci.* **27**, 13420–13429 (2007).

52. F. Pouille, M. Scanziani, Routing of spike series by dynamic circuits in the hippocampus. *Nature* **429**, 717–723 (2004).

53. V. S. Sohal, F. Zhang, O. Yizhar, K. Deisseroth, Parvalbumin neurons and gamma rhythms enhance cortical circuit performance. *Nature* **459**, 698–702 (2009).

54. J. A. Cardin *et al.*, Driving fast-spiking cells induces gamma rhythm and controls sensory responses. *Nature* **459**, 663–667 (2009).

55. G. Liu, R. W. Tsien, Synaptic transmission at single visualized hippocampal boutons. *Neuropharmacology* **34**, 1407–1421 (1995).

56. S. Leow-Dyke *et al.*, Neuronal Toll-like receptor 4 signaling induces brain endothelial activation and neutrophil transmigration in vitro. *J. Neuroinflammation* **9**, 230 (2012).

57. A. Alsina *et al.*, Real-time subpixel-accuracy tracking of single mitochondria in neurons reveals heterogeneous mitochondrial motion. *Biochem. Biophys. Res. Commun.* **493**, 776–782 (2017).

58. C. Park *et al*, Unique dynamics and exocytosis properties of GABAergic synaptic vesicles revealed by three-dimensional single vesicle tracking (NYU Dataset). NYU Data Catalog. https://datacatalog.med.nyu.edu/dataset/10426. Deposited 8 January 2021.

Park et al.
Unique dynamics and exocytosis properties of GABAergic synaptic vesicles revealed by three-dimensional